Available online at website: https://journal.bcrec.id/index.php/bcrec

Bulletin of Chemical Reaction Engineering & Catalysis, 21 (3) 2026, 500-506

Original Research Article

Recovery of Gold Nanoparticles from Aqueous Solutions via Hydrogen Peroxide Reduction using Self-Propelled Palm Shell-Supported Manganese Dioxide Composites

Muhammad Irsyad Roslan[1], Nor Hasanah Zubaidi[1], Chan Juinn Chieh Derek[2], Eric D. van Hullebusch[3], Siu Hua Chang[1*]

[1]*Waste Management and Resource Recovery (WeResCue) Group, Faculty of Chemical Engineering, Universiti Teknologi MARA, Cawangan Pulau Pinang, 13500 Permatang Pauh, Penang, Malaysia.*

[2]*School of Chemical Engineering, Engineering Campus, Universiti Sains Malaysia, 14300 Nibong Tebal, Pulau Pinang, Malaysia.*

[3]*Université Paris Cité, Institute de Physique du Globe de Paris, CNRS, Paris, France.*

Received: 22th January 2026; Revised: 9th March 2026; Accepted: 10th March 2026
Available online: 16th March 2026; Published regularly: October 2026

Abstract

Intensive mechanical stirring, commonly used for gold nanoparticle (AuNP) recovery, suffers from drawbacks such as mechanical wear and high operational costs. Self-propelled catalytic composites capable of autonomous motion present a promising alternative, yet their applicability and influence on AuNP recovery efficiency remain insufficiently explored. Hence, this study aimed to fabricate palm shell-supported manganese dioxide (MnO_2) composites and investigate the effect of their dosage on AuNP recovery via hydrogen peroxide reduction. The composites were characterized using Field Emission Scanning Electron Microscopy with Energy Dispersive X-Ray Spectroscopy (FESEM-EDX) to assess their morphology, particle size, and elemental composition, while UV-Vis spectroscopy was used to monitor AuNP formation through localized surface plasmon resonance (LSPR) responses. Results revealed that a composite dosage of 0.2 g/L produced the sharpest LSPR peak at 530 nm, indicating the highest yield of spherical AuNPs with particle sizes ranging from 20 to 80 nm. Motion analysis showed that the composites exhibited autonomous bubble-propelled motion at an average speed of 25.5 µm/s, following linear and semi-circular trajectories that enhanced mass transfer and AuNP recovery efficiency. Overall, palm shell-supported MnO_2 composites demonstrate great potential as an alternative to conventional mechanical stirring-based methods for recovering AuNPs.

Keywords: Gold nanoparticles; self-propelled catalytic composites; hydrogen peroxide; manganese dioxide; palm shell

How to Cite: Roslan, M. I., Zubaidi, N. H., Derek, C. J. C., van Hullebusch, E. D., Chang, S. H. (2026). Recovery of Gold Nanoparticles from Aqueous Solutions via Hydrogen Peroxide Reduction using Self-Propelled Palm Shell-Supported Manganese Dioxide Composites. *Bulletin of Chemical Reaction Engineering & Catalysis*, 21 (3), 500-506. (DOI: 10.9767/bcrec.20628)

Permalink/DOI: https://doi.org/10.9767/bcrec.20628

1. Introduction

Gold nanoparticles (AuNPs) have gained considerable attention across various scientific and industrial fields due to their unique optical properties, which distinguish them from other metals. These properties arise from their ability to interact with light through localized surface plasmon resonance (LSPR) [1–3]. In addition, AuNPs are easy to synthesize, can be readily surface-modified, and exhibit excellent colloidal stability, making them highly suitable for medical applications such as diagnostics, therapeutics, and drug delivery [2,4,5]. From a sustainability perspective, AuNPs can be recovered from gold complexes in aqueous solutions [6–9] typically obtained by leaching secondary sources such as e-waste and spent catalyst, followed by separation and purification using different techniques [10,11]. Among the available recovery methods [3,12–15], chemical reduction using hydrogen

* Corresponding Author.
Email: shchang@uitm.edu.my (S. H. Chang)

peroxide (H_2O_2) has proven particularly effective in reducing Au^{3+} to Au^0 from $AuCl_4^-$ complexes, while being cost-efficient and generating no harmful byproducts [16–19].

Like many heterogenous chemical reactions, efficient fluid mixing is crucial to enhance reaction rates and gold recovery during reduction. However, mechanical stirring is known for being problematic, wear and tear over time, the need for regular maintenance, and producing significant heat during long-hour operations which results in high operational cost. To address these challenges, self-propelled, chemically powered catalytic composites have emerged as a promising alternative, offering autonomous mixing and enhanced reaction efficiency without mechanical input [20]. Biomass-based materials are ideal support for such composites, as they are abundant, inexpensive and easy to process [21,22], and exhibit high adsorption capacity when pyrolyzed. In this study, palm shell, an abundant biomass resource in Malaysia [23], was selected as the support material due to its rigid and highly porous structure, which allows for effective catalyst immobilization [24]. Manganese dioxide (MnO_2) was chosen as the catalytic component due to its ability to decompose H_2O_2 into water and oxygen gas bubbles, which drive composite propulsion and improve AuNP recovery efficiency [25,26].

To date, only a limited number of studies have explored the use of self-propelled catalytic composites for metal recovery from aqueous solutions [20]. For instance, iron/platinum-based self-propelled composites activated by H_2O_2, serving both reagent and fuel, have been employed to treat organic pollutants in wastewater [25]. However, research on using self-propelled composites specifically for AuNP recovery remains scarce and has thus far been reported only by Srivistana *et al*. [26]. However, the use of platinum-based support materials is costly. In contrast, palm shell offers a significantly cheaper and more environmentally friendly alternative, making it a more sustainable option for research. Furthermore, studies on the motion performance of micro scavengers in AuNPs recovery remain underexplored and will therefore be a key focus of this work.

Therefore, this study aimed to fabricate palm shell-supported MnO_2 composites and evaluate their effectiveness in recovering AuNPs from aqueous solutions. The specific objectives include: (i) fabricating palm shell-supported MnO_2 composites, and (ii) investigating the effects of composite dosage on AuNPs recovery. The composites were characterized by Field Emission Scanning Electron Microscopy with Energy Dispersive X-Ray Spectroscopy (FESEM-EDX) to determine their morphology, size and elemental composition. The effectiveness of the composites in AuNP recovery was assessed by analysing their LSPR peaks using a UV-vis spectrophotometer. Additionally, the motion behavior and speed of the composites were examined under a microscope and quantified using Image J software.

2. Materials and Method

2.1 Materials

Palm shell biochar was provided by Malaysian Palm Oil Board (MPOB). Gold (III) chloride solution ($HAuCl_4$, 30 wt% in dilute HCl) was supplied from Sigma-Aldrich with analytical grade purity. Hydrogen peroxide (H_2O_2, 30-32%), and sodium hydroxide pellets (NaOH) were purchased from Quality Reagent Chemical (QRec). Potassium permanganate powder ($KMnO_4$) and polyvinyl alcohol powder (PVA) were supplied from R&M Chemicals.

2.2 Fabrication of Palm Shell-supported MnO_2 Composites

Palm shell biochar was crushed using mortar and pestle into fine particles, then sieved with 120 mesh into 125 um powder. 1 gram of palm shell biochar powder was immersed in 100 mL of deionized water and ultrasonicated for 5 minutes. 1 gram of $KMnO_4$ powder was added into the solution and stirred overnight for 24 hours. Afterward, the mixed solution was filtered using vacuum filtration, and the newly coated powder was rinsed with distilled water. The powder was then dried in an oven at 105 ^oC for 24 hours.

2.3 Recovery of AuNPs from Gold Aqueous Solution using Palm Shell Supported MnO_2 Composites

Specifically, 25 mL of 0.50 mM of gold solution was prepared from stock solution ($HAuCl_4$). A clear 1 M of PVA solution was prepared by constant heating PVA pellets at 80 ^oC and then added into the gold solution. Dosages of 0.1 g/L palm shell-supported MnO_2 composites were added into the mixture. Afterwards, 5 mL of 1 M of H_2O_2 was added into the solution drop by drop, and the color changes were observed after 10 minutes. This experiment was repeated with different dosages of palm shell-supported MnO_2 (0.2, 0.3, 0.4 and 0.5 g/L).

2.4 Characterization Methods

Different aqueous colloidal AuNP samples were subjected to UV-Vis Spectrophotometry (Cary 60, Agilent) analysis to measure their LSPR peaks. Disposable plastic cuvettes were used to hold the AuNP samples during the analysis to prevent adhesion of the nanoparticles. The presence of gold nanoparticles was confirmed by their LSPR absorption band in the range of 510 –

600 nm. Surface morphology and elemental distribution of palm shell-supported MnO_2 composites were examined by field emission scanning electron microscopy and energy-dispersive X-ray analysis (FESEM-EDX, Thermo Fisher Scientific, Quanta 450 FEG). The motion behavior and trajectory of the palm shell-supported MnO_2 composites were examined under an Olympus BX53 microscope, and their speed and movement patterns were quantitatively analysed using Image J software.

3. Results and Discussion

3.1. Morphology, Composition and Structure of Palm Shell-supported MnO_2 Composites

The morphology, structure and composition of the palm shell-supported MnO_2 composites were analyzed using FESEM coupled with EDX. This analysis aimed to confirm the successful formation of palm shell-supported MnO_2 composites, consistent with previous related studies. As shown in Figure 1 (a), the composite shows a highly porous surface structure, typical of pyrolyzed biomass materials. This porosity is due to the release of volatile organic compounds during pyrolysis, which leaves behind numerous voids and channels in the carbonaceous structure. These pores play a important role in facilitating ion transport and enhancing the surface area of the composites [27]. Similarly, Abnisa *et al.* [29] reported that palm shell-based biochar with a rich porous structure exhibits high absorption capacity for methylene blue molecules.

Additionally, the MnO_2 nanoparticles were observed to be well-dispersed and anchored within the pores on the surface of the palm shell biochar. This confirms the successful formation and strong surface interaction between MnO_2 and the palm shell support. Previous studies have also demonstrated uniform MnO_2 deposition on other types of biochar such as rice husk [28], coconut shell [29], and peanut shell [30]. This behavior is due to superior specific surface area and excellent pore structure of biochar, which promotes the uniform dispersion of MnO_2 nanoparticles [31], as observed for the palm shell-supported MnO_2 in this work. The observed uneven and rough surface texture may result from partial agglomeration of MnO_2 nanoparticles during synthesis. It is generally known that smaller MnO_2 particles exhibit higher catalytic activity compared to larger aggregates [32].

The elemental composition of the palm shell-supported MnO_2 composites was further verified by EDX analysis, as shown in Figure 1 (b). The EDX spectra revealed the presence of carbon (C) (79.94 wt%), oxygen (O) (13.57 wt%), manganese (Mn) (4.99 wt%), and potassium (K) (1.49 wt%). The high carbon content originates from the palm shell biochar, which is inherently rich in organic carbon. The existence of element K is due to the reduction of $KMnO_4$ during MnO_2 formation, releasing K^+ ions in the process. The presence of elements Mn and O confirmed the successful synthesis and deposition of MnO_2 nanoparticles on the palm shell surface. Overall, these findings confirm that the fabrication of palm shell-supported MnO_2 composites was successful, producing a material with a porous biochar matrix effectively decorated with MnO_2 nanoparticles.

3.2. Effect of Palm Shell-supported MnO_2 Composite Dosage on AuNP Recovery from Aqueous Gold Solutions

The effect of palm shell-supported MnO_2 composite dosage (0.1, 0.2, 0.3, 0.4 and 0.5 g/L) on the recovery of AuNPs from aqueous gold solutions was evaluated using UV-vis spectrophotometry. Previous studies have shown that variations in composite dosages can significantly influence their metal recovery performance [33]. As shown in Figure 2 (a). the color of the recovered AuNP suspensions ranged from purplish to reddish, which is characteristic of colloidal AuNPs, consistent with previous studies

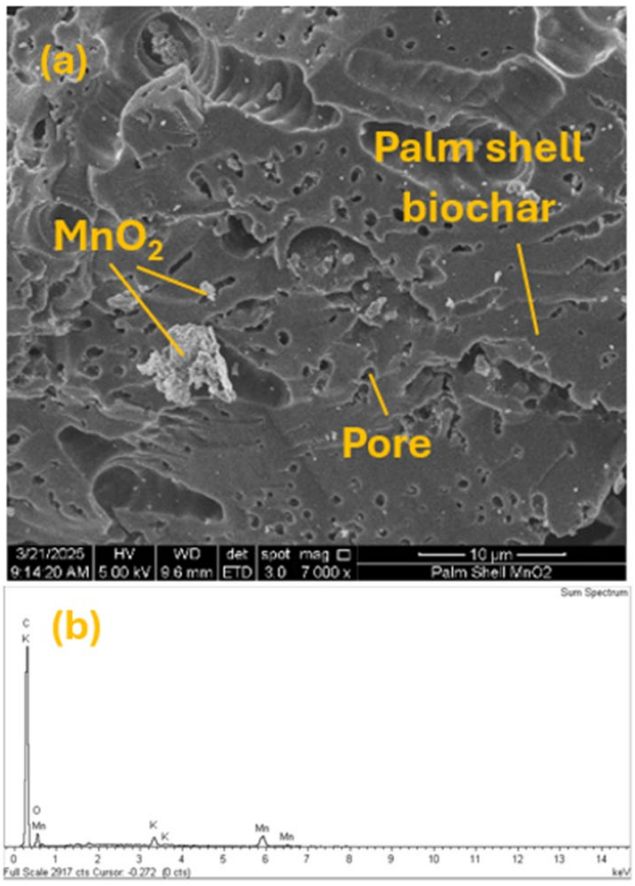

Figure 1. FESEM images of (a) palm shell-supported MnO_2 composites showing the porous palm shell biochar surface and MnO_2 particle dispersion, and (b) the corresponding EDX spectrum confirming the elemental composition of palm shell-supported MnO_2 composites.

[16,17,34]. This observation was further confirmed by the LSPR spectra in Figure 2 (b), where the absorption peaks appeared between 525 and 535 nm, confirming the successful formation of AuNPs [35]. The peak intensity increased sharply as the composite dosage rose from 0.1 g/L to 0.2 g/L, showing a prominent peak at 525 nm. This peak indicates AuNP with size range of 20-80 nm. This enhancement can be attributed to the improved catalytic decomposition of H_2O_2 by MnO_2 into H_2O and O_2, as represented by Equation (1) [36]. The rapid decomposition of H_2O_2 generates electrons, which facilitate the reduction of Au^{3+} to metallic Au^0 [17]:

$$2H_2O_2\,(l) \xrightarrow{MnO_2} 2H_2O\,(l) + O_2\,(g) \qquad (1)$$

However, beyond 0.2 g/L, the LSPR peaks gradually decreased up to 0.5 g/L. This decline may result from excessive decomposition of H_2O_2, which generates an abundance of O_2 bubbles that obstruct access to active catalytic sites of MnO_2 [37,38], thereby hindering the mass transfer of Au^{3+} ions. Another possible explanation is mechanical attrition of the composites caused by frequent collisions or chaotic motion induced by vigorous bubble propulsion. Such interactions can lead to agglomeration or fragmentation of the composites, reducing the number of available active sites and ultimately diminishing MnO_2 catalytic activity [39,40].

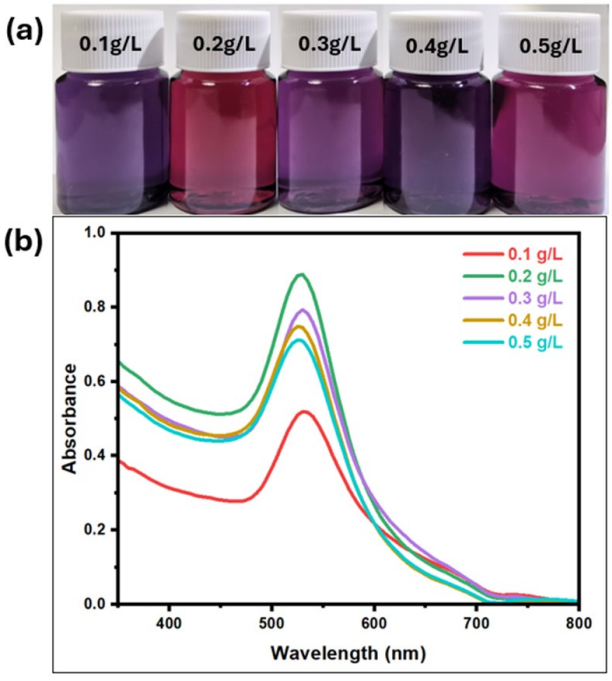

Figure 2. Effect of palm shell-supported MnO_2 dosage on (a) the color of AuNP suspensions and (b) UV-vis LSPR peaks recorded at 0.1-0.5 g/L in a 0.5 mM $HAuCl_4$ solution containing 1.0 M H_2O_2 and 2% PVA with pH of 6.5.

Meanwhile, LSPR can indicate the presence of colloidal AuNPs and provide an estimation of their shape and size, it should only be considered semi-quantitative. More reliable quantitative data, such as from inductively coupled plasma (ICP) analysis, are required to determine the percentage of Au(III) reduced. As this study mainly focuses on the LSPR trends at different composite dosages, quantitative recovery data of reduced Au(III) is recommended for future studies to further verify the reduction efficiency.

3.3. Motion Analysis of Palm Shell-supported MnO_2 Composites

Typical time-lapse images captured from the videos of the moving palm shell-supported MnO_2 composites in a 0.5 mM $HAuCl_4$ solution containing 1 M H_2O_2 and 2% PVA, are presented in Figure 3. In this video, a single particle of palm shell-supported MnO_2 composites was tracked and three independent replicates were conducted to determine the average speed, with a % RSD of less than 5%. The figure shows that composites propel themselves autonomously in presence of H_2O_2 as fuel, achieving an average speed of 25.507 µm/s. This autonomous motion is attributed to the synergistic interaction between palm shell and MnO_2, as well as the large catalytic area provided by the hierarchically porous and rough inner surface of the composites, which enhances the decomposition of H_2O_2.

Different motion patterns were observed during the experiment. At 10 and 60 seconds, the composites exhibited semi-circular trajectories, at 20, 40 and 50 seconds, they displayed linear motion. This behavior is due to the rapid decomposition of H_2O_2 at MnO_2 sites, releasing

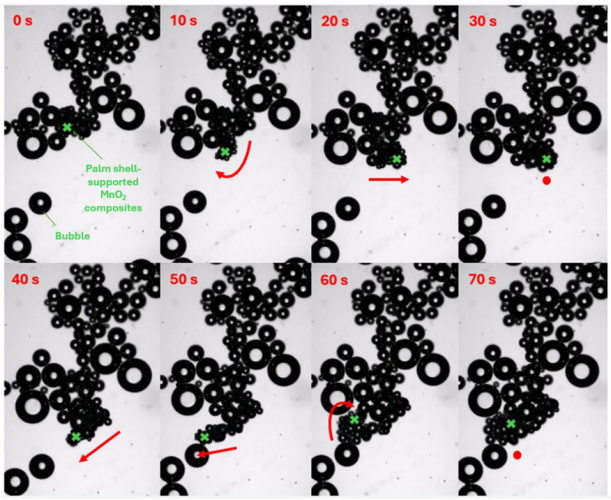

Figure 3. Time-lapse images depicting the propulsion behavior of 0.2 g/L palm shell-supported MnO_2 composites in a 0.5 mM $HAuCl_4$ solution containing 1 M H_2O_2 and 2% PVA, with pH of 6.5 recorded over a period of 0 to 70 seconds.

multiple small oxygen bubbles that generate thrust in the opposite directions. However, no notable movement was observed at 30 and 70 seconds, possibly due to an uneven distribution of MnO_2 catalytic sites, leading to non-uniform bubble release in multiple directions simultaneously. In addition, the size and frequency of bubbles significantly affect the motion trajectory and speed. Previous studies have shown that as H_2O_2 concentration rises, the bubble sizes increase while the bubble release frequency decreases [41]. Larger bubbles hinder free motion by increasing drag, while a lower bubble frequency provides results in reduced thrust, thereby decreasing the propulsion speed of the composites.

The surfactant concentration also influences composite motion. At high surfactant concentrations, fluid viscosity increases, leading to greater vicious resistance and reduced speed [42]. A related study reported that increasing SDS concentration from 5% to 15% reduced composite speed from 572 μm/s to approximately 200 μm/s [41]. However, no clear correlation between the speed and the motion behavior of composites has been established to date. Hence, further optimization of H_2O_2-to-surfactant ratio is recommended for future work. Despite these variations, the results conclusively demonstrate that the palm shell-supported MnO_2 composites are capable of autonomous, bubble-propelled motion driven by H_2O_2 decomposition, thereby supporting the hypothesis of this study.

4. Conclusions

In summary, palm shell-supported MnO_2 composites have been successfully prepared through an in-situ chemical precipitation process. The excellent porosity of palm shell biochar provides a strong anchoring surface for MnO_2 formation. The decomposition of H_2O_2 over the MnO_2 catalyst facilitates rapid electron distribution in the reaction medium for the reduction of Au^{3+} ions to Au^0, while simultaneously enhancing mass transfer through oxygen bubble propulsion. The synthesized AuNP exhibited purplish to reddish coloration, consistent with reports in the literature. The LSPR wavelengths of AuNPs recovered with different palm shell-supported MnO_2 dosages fell within the range of 525 - 535 nm, aligning well with the characteristic range typically observed for AuNPs. Furthermore, the 0.2 g/L composites dosage produced the highest LSPR peak intensity, which decreased at higher dosages (up to 0.5 g/L), possibly due to excessive motion of the MnO_2 composites leading to partial catalyst deactivation. Various motion patterns, including semi-circular and linear trajectories, were observed for the palm shell-supported MnO_2 composites, which moved at an average speed of 25.507 μm/s. The irregular frequency and size of the generated oxygen bubbles may have contributed to the inconsistencies in particle motion. A higher PVA concentration could also increase the overall viscosity of the medium, thereby reducing propulsion speed. Nevertheless, the motion and speed can be further optimized by adjusting the ratio of H_2O_2 to surfactant in future studies. Overall, this work has successfully achieved its objective by fabricating palm shell-supported MnO_2 composites, recovering AuNPs from aqueous gold solutions via H_2O_2 reduction, and confirming their motion behavior under microscopic observation.

Acknowledgment

This study was funded by Universiti Teknologi MARA (UiTM) through the Strategic Research Partnership grant (100-RMC 5/3/SRP (108/2022)) and supported in part by the UiTM Conference Support Fund. Additionally, the research project received funding from the French government via the Embassy of France in Malaysia and the myTIGER program (MT30-06/2022), contributing to its success.

CRedit Author Statement

Author Contributions: M.I Roslan: Conceptualization, Methodology, Investigation, Writing Original Draft, Writing, Review and Editing, Visualization; N. H Zubaidi: Methodology, Investigation; C. J. C. Derek: Supervision, Resources, Funding acquisition, Review and Editing; Eric D.van Hullebusch: Resources, Funding acquisition, Review and Editing; S.H. Chang: Conceptualization, Validation, Writing, Review and Editing, Supervision, Funding acquisition. All authors have read and agreed to the published version of the manuscript.

References

[1] Connor, D.M., Broome, A.M. (2018). Gold Nanoparticles for the Delivery of Cancer Therapeutics. *Advances in Cancer Research*, 139, 163–184. DOI: 10.1016/BS.ACR.2018.05.001.

[2] Nejati, K., Dadashpour, M., Gharibi, T., Mellatyar, H., Akbarzadeh, A. (2022). Biomedical Applications of Functionalized Gold Nanoparticles: A Review. *Journal of Cluster Science*, 33(1), 1-16. DOI: 10.1007/s10876-020-01955-9.

[3] Hammami, I., Alabdallah, N.M., jomaa, A. Al, kamoun, M. (2021). Gold nanoparticles: Synthesis properties and applications. *Journal of King Saud University – Science*, 33(29), 101560. DOI: 10.1016/j.jksus.2021.101560.

[4] Grzelczak, M., Pérez-Juste, J., Mulvaney, P., Liz-Marzán, L.M. (2008). Shape control in gold nanoparticle synthesis. *Chemical Society Reviews*, 37(9), 1783–1791. DOI: 10.1039/b711490g.

[5] Madkour, L.H. (2018). Applications of gold nanoparticles in medicine and therapy. *Pharmacy & Pharmacology International Journal*, 6(3), 157-174. DOI: 10.15406/ppij.2018.06.00172.

[6] Huy Do, M., Tien Nguyen, G., Dong Thach, U., Lee, Y., Huu Bui, T. (2023). Advances in hydrometallurgical approaches for gold recovery from E-waste: A comprehensive review and perspectives. *Minerals Engineering*, 191(3), 107977. DOI: 10.1016/j.mineng.2022.107977.

[7] Sahu, S., Mohapatra, M., Devi, N. (2022). Effective hydrometallurgical route for recovery of energy critical elements from E-wastes and future aspects. *Materials Today Proceedings*, 67(8), 1016-1023. DOI: 10.1016/j.matpr.2022.05.491.

[8] Panda, R., Dinkar, O.S., Kumari, A., Gupta, R., Jha, M.K., Pathak, D.D. (2021). Hydrometallurgical processing of waste integrated circuits (ICs) to recover Ag and generate mix concentrate of Au, Pd and Pt. *Journal of Industrial and Engineering Chemistry*, 93, 315–321. DOI: 10.1016/j.jiec.2020.10.007.

[9] Gökelma, M., Birich, A., Stopic, S., Friedrich, B. (2016). A Review on Alternative Gold Recovery Re-agents to Cyanide. *Journal of Materials Science and Chemical Engineering*, 04(08), 8–17. DOI: 10.4236/msce.2016.48002.

[10] Chang, S.H., Jampang, A.O.A., Din, A.T.M. (2025). Adsorption isotherms, kinetics, and thermodynamics of Au(III) on chitosan/palm kernel fatty acid distillate/magnetite nanocomposites. *International Journal of Biological Macromolecules*, 304(1), 140913. DOI: 10.1016/j.ijbiomac.2025.140913.

[11] Chang, S.H., Jampang, A.O.A. (2021). Green extraction of gold(III) and copper(II) from chloride media by palm kernel fatty acid distillate. *Journal of Water Process Engineering*, 43, 102298. DOI: 10.1016/j.jwpe.2021.102298.

[12] Daruich De Souza, C., Ribeiro Nogueira, B., Rostelato, M.E.C.M. (2019). Review of the methodologies used in the synthesis gold nanoparticles by chemical reduction. *Journal of Alloys and Compounds*, 798, 714–740. DOI: 10.1016/j.jallcom.2019.05.153.

[13] Manigandan, S., Rajmohan, K.S., Varjani, S. (2020). Current trends in gold recovery from electronic wastes. *Current Developments in Biotechnology and Bioengineering: Resource Recovery from Wastes*, 307–325. DOI: 10.1016/B978-0-444-64321-6.00016-1.

[14] Makertihartha, I.G.B.N., Zunita, M., Rizki, Z., Dharmawijaya, P.T. (2017). Solvent extraction of gold using ionic liquid based process. *AIP Conference Proceedings*. 1805(1), 030008. DOI: 10.1063/1.4974419.

[15] Grosse, A.C., Dicinoski, G.W., Shaw, M.J., Haddad, P.R. (2003). Leaching and recovery of gold using ammoniacal thiosulfate leach liquors (a review). *Hydrometallurgy*, 69 (1-3), 1-21. DOI: 10.1016/S0304-386X(02)00169-X.

[16] Li, Q., Lu, B., Zhang, L., Lu, C. (2012). Synthesis and stability evaluation of size-controlled gold nanoparticles via nonionic fluorosurfactant-assisted hydrogen peroxide reduction. *Journal of Materials Chemistry*, 22(27), 13564-13570. DOI: 10.1039/c2jm31528a.

[17] Panda, B.R., Chattopadhyay, A. (2007). Synthesis of Au nanoparticles at "all" pH by H2O2 reduction of HAuCl4. *Journal of Nanoscience and Nanotechnology*, 7(6), 1911–1915. DOI: 10.1166/jnn.2007.740.

[18] Sarma, T.K., Chowdhury, D., Paul, A., Chattopadhyay, A. (2002). Synthesis of Au nanoparticle-conductive polyaniline composite using H2O2 as oxidising as well as reducing agent. *Chemical Communications*, 2(10), 1048–1049. DOI: 10.1039/b201014c.

[19] Li, Q., Lu, B., Zhang, L., Lu, C. (2012). Synthesis and stability evaluation of size-controlled gold nanoparticles via nonionic fluorosurfactant-assisted hydrogen peroxide reduction. *Journal of Materials Chemistry*, 22(27), 13564–13570. DOI: 10.1039/c2jm31528a.

[20] Chang, S.H. (2022). Micro/nanomotors for metal ion detection and removal from water: A review. *Materials Today Sustainability*, 19, 100196. DOI: 10.1016/j.mtsust.2022.100196.

[21] Halim, S.F.A., Chang, S.H., Morad, N. (2020). Extraction of Cu(II) ions from aqueous solutions by free fatty acid-rich oils as green extractants. *Journal of Water Process Engineering*, 33, 100997. DOI: 10.1016/j.jwpe.2019.100997.

[22] Abdul Halim, S.F., Chang, S.H., Morad, N. (2019). Parametric studies of Cu(II) ion extraction into palm kernel fatty acid distillate as a green organic solvent. *Journal of Environmental Chemical Engineering*, 7(6), 103488. DOI: 10.1016/j.jece.2019.103488.

[23] Hosseini, S.E., Wahid, M.A. (2014). Utilization of palm solid residue as a source of renewable and sustainable energy in Malaysia. *Renewable and Sustainable Energy Reviews*, 40, 621–632. DOI: 10.1016/j.rser.2014.07.214.

[24] Prasetyo, I., Mukti, N.I.F., Cahyono, R.B., Prasetya, A., Ariyanto, T. (2020). Nanoporous Carbon Prepared from Palm Kernel Shell for CO2/CH4 Separation. *Waste and Biomass Valorization*, 11(10), 5599–5606. DOI: 10.1007/s12649-020-01006-4.

[25] Soler, L., Magdanz, V., Fomin, V.M., Sanchez, S., Schmidt, O.G. (2013). Self-propelled micromotors for cleaning polluted water. *ACS Nano*, 7(11), 9611–9620. DOI: 10.1021/nn405075d.

[26] Srivastava, S.K., Medina-Sánchez, M., Schmidt, O.G. (2017). Autonomously propelled microscavengers for precious metal recovery. *Chemical Communications*, 53(58), 8140–8143. DOI: 10.1039/c7cc02605f.

[27] Yuan, C., Lin, H., Lu, H., Xing, E., Zhang, Y., Xie, B. (2016). Synthesis of hierarchically porous MnO2/rice husks derived carbon composite as high-performance electrode material for supercapacitors. *Applied Energy*, 178, 260–268. DOI: 10.1016/j.apenergy.2016.06.057.

[28] Cuong, D.V., Wu, P.C., Chen, L.I., Hou, C.H. (2021). Active MnO2/biochar composite for efficient As(III) removal: Insight into the mechanisms of redox transformation and adsorption. *Water Research*, 188, 116495. DOI: 10.1016/j.watres.2020.116495.

[29] Fang, X., Wu, Y., Xu, L., Gan, L. (2022). Fast removal of bisphenol A by coconut shell biochar incorporated α-MnO2 composites via peroxymonosulfate activation. *Journal of Water Process Engineering*, 49, 103071. DOI: 10.1016/j.jwpe.2022.103071.

[30] Wang, H., Wang, A., Ji, J., Zhang, X., Wang, Y., Zhang, W., Wang, Y., Wang, H., Song, Y., Liu, Q. (2024). Study on the adsorption performance of manganese dioxide loaded modified biochar composite materials for cadmium ions (Ⅱ) in solution. *Research Square Preprint*. DOI: 10.21203/rs.3.rs-4419330/v1.

[31] Chen, H., Li, X., Li, W., Feng, J., Zhao, Y., Zhang, H., Ren, Y. (2024). Nitrogen-doped biochar/MnO2 as an efficient PMS activator for synergistic BPA degradation via non-free radical pathways in the water. *Journal of Environmental Chemical Engineering*, 12(2), 122446. DOI: 10.1016/j.jece.2024.112446.

[32] Dassanayake, R.S., Rajakaruna, E., Abidi, N. (2019). Borax-cross-linked guar gum-manganese dioxide composites for oxidative decolorization of methylene blue. *Journal of Nanomaterials*, 2019, 7232715. DOI: 10.1155/2019/7232715.

[33] Benettayeb, A., Morsli, A., Elwakeel, K.Z., Hamza, M.F., Guibal, E. (2021). Recovery of heavy metal ions using magnetic glycine-modified chitosan—application to aqueous solutions and tailing leachate. *Applied Sciences (Switzerland)*, 11(18), 8377. DOI: 10.3390/app11188377.

[34] Liu, X., Xu, H., Xia, H., Wang, D. (2012). Rapid seeded growth of monodisperse, quasi-spherical, citrate-stabilized gold nanoparticles via H2O2 reduction. *Langmuir*, 28(38), 13720–13726. DOI: 10.1021/la3027804.

[35] Jin, Y., Wang, P., Yin, D., Liu, J., Qin, L., Yu, N., Xie, G., Li, B. (2007). Gold nanoparticles prepared by sonochemical method in thiol-functionalized ionic liquid. *Colloids and Surfaces A: Physicochemical and Engineering Aspects*, 302(1–3), 366–370. DOI: 10.1016/j.colsurfa.2007.02.060.

[36] Dolhun, J.J. (2014). Observations on manganese dioxide as a catalyst in the decomposition of hydrogen peroxide: A safer demonstration. *Journal of Chemical Education*, 91(5), 760–762. DOI: 10.1021/ed4006826.

[37] Xu, S., Liu, H., Zheng, N., Tao, H.B. (2024). Physical Degradation of Anode Catalyst Layer in Proton Exchange Membrane Water Electrolysis. *Advance Materials Interfaces*, 12(4), 2400549. DOI: 10.1002/admi.202400549.

[38] Xu, P., Bernal-Juan, F.D., Lefferts, L. (2021). Effect of oxygen on formic acid decomposition over Pd catalyst. *Journal of Catalysis*, 394, 342–352. DOI: 10.1016/j.jcat.2020.10.032.

[39] Bartholomew, C.H. (2001). Mechanisms of catalyst deactivation. *Applied Catalysis A: General*, 212(1-2), 17-60. DOI: 10.1016/S0926-860X(00)00843-7.

[40] Thon, A., Werther, J. (2010). Attrition resistance of a VPO catalyst. *Applied Catalysis A: General*, 376(1), 56–65. DOI: 10.1016/j.apcata.2009.11.036.

[41] Ye, H., Kang, J., Ma, G., Sun, H., Wang, S. (2018). High-speed graphene@Ag-MnO2 micromotors at low peroxide levels. *Journal of Colloid and Interface Science*, 528, 271–280. DOI: 10.1016/j.jcis.2018.05.088.

[42] Asari, M. (2013). Effects of Surfactant on Bubble Size Distribution and Gas Hold-up in a Bubble Column. *American Journal of Chemical Engineering*, 1(2), 50. DOI: 10.11648/j.ajche.20130102.14.